Science Advances

AAAS

advances.sciencemag.org/cgi/content/full/4/3/eaaq0504/DC1

Supplementary Materials for

The limits of earthquake early warning: Timeliness of ground motion estimates

Sarah E. Minson, Men-Andrin Meier, Annemarie S. Baltay, Thomas C. Hanks, Elizabeth S. Cochran

Published 21 March 2018, *Sci. Adv.* **4**, eaaq0504 (2018)
DOI: 10.1126/sciadv.aaq0504

The PDF file includes:

Other Supplementary Material for this manuscript includes the following:
(available at advances.sciencemag.org/cgi/content/full/4/3/eaaq0504/DC1)

- data file S1 (Microsoft Excel format). Description of the 48,841 seismograms used in this study.

- movie S1 (.mp4 format). Evolution of observed and predicted PGA values for finite fault scenario presented in Fig. 5.

Supplementary Materials

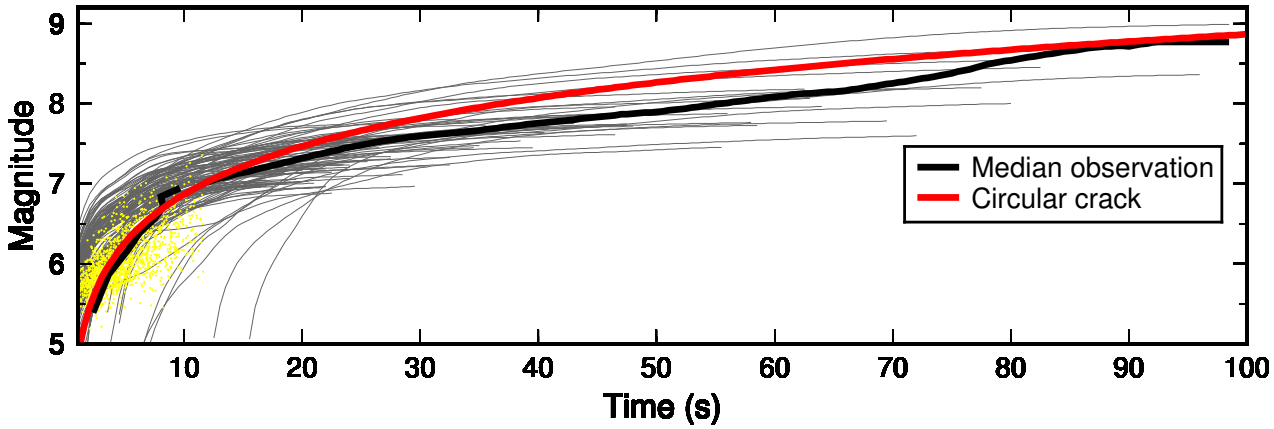

fig. S1. Observed and theoretical evolution of moment release. Comparison of moment release for a circular crack (eq. 1) with observed cumulative moment for 115 **M**≥7 subduction zone earthquakes (grey lines) (23) and catalog of corner frequencies for **M**<7 earthquakes (39). Black line is median of (23) for **M**≥7 and median of (39) for **M**<7.

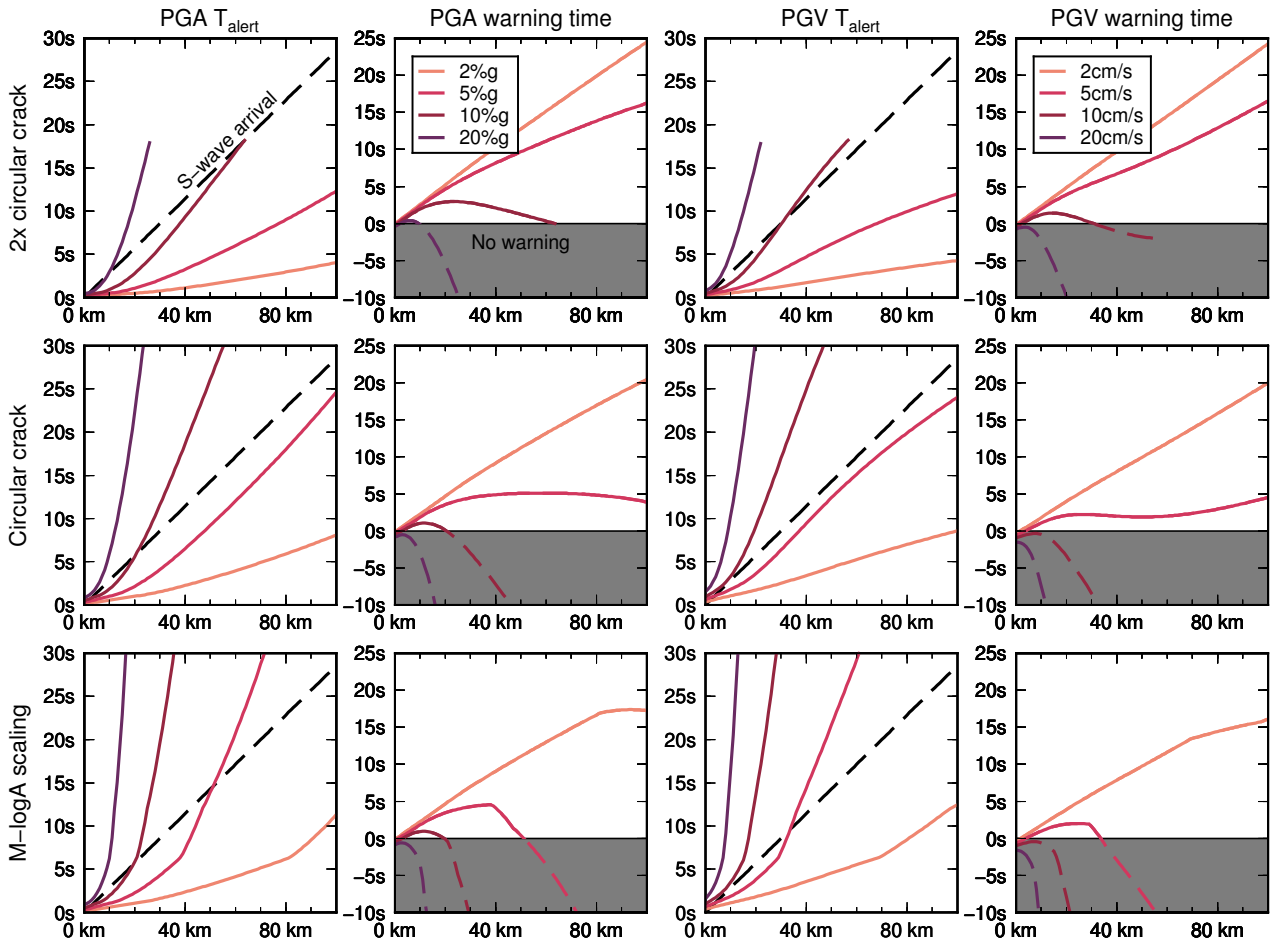

fig. S2. Comparison of alert and warning times for PGA and PGV. Same as Fig. 4 for each of the three source-time functions presented in Fig. 3C (top to bottom: estimating moment release twice as fast as a circular crack, estimate moment release at the same rate as a circular crack, and 15-km-wide rupture propagating at 3 km/s whose moment is given by the magnitude-log area scaling of (29)). The left two columns are for users who wish to receive alerts for accelerations exceeding 2, 5, 10, or 20%*g*. The right two columns are for users who wish to receive alerts for

ground velocities exceeding 2, 5, 10, or 20 cm/s. Both sets of thresholds are approximately equivalent to Modified Mercalli Intensity (MMI) IV-VII.

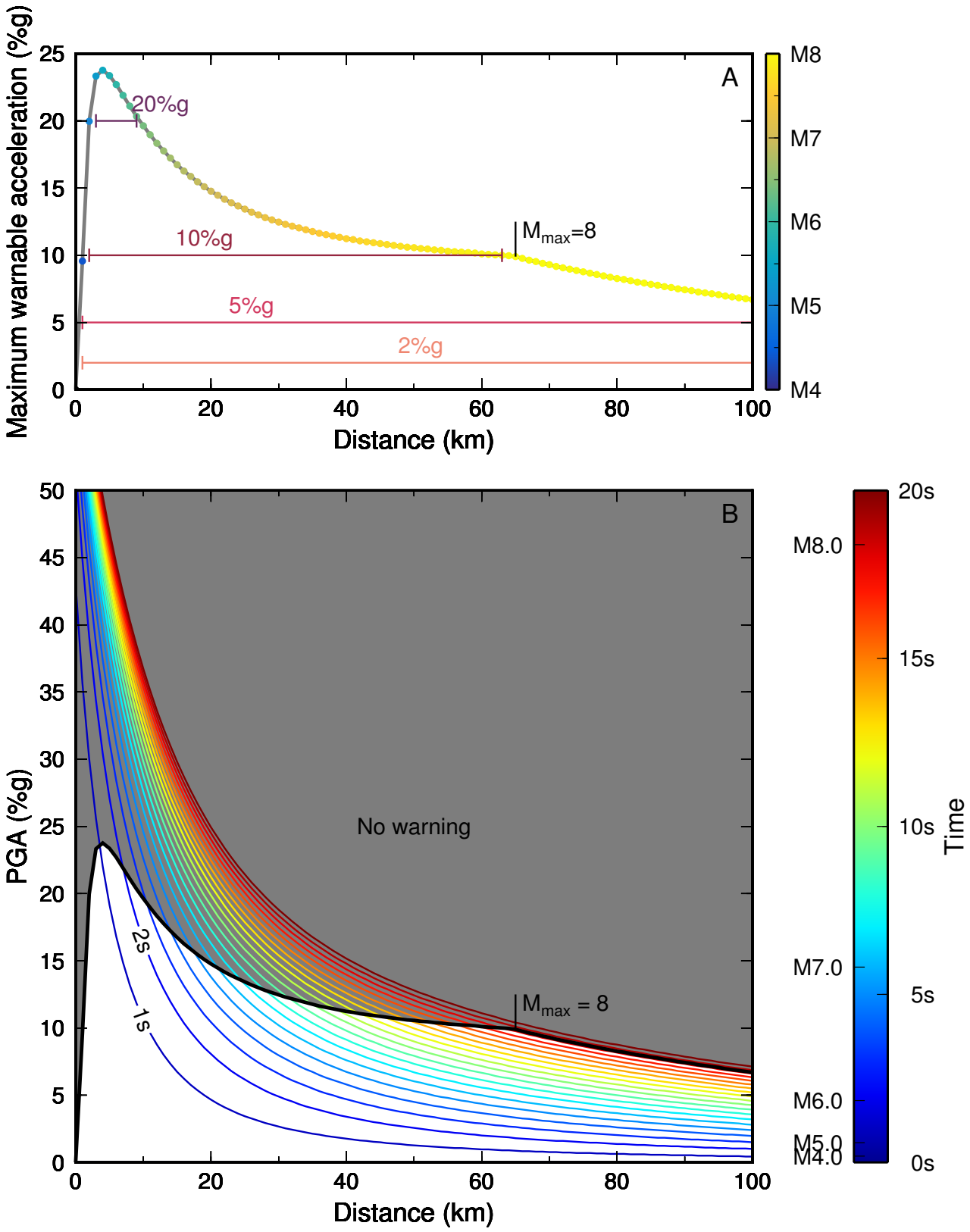

fig. S3. Time evolution of predicted PGA for a point source and maximum warnable acceleration. (A) Maximum acceleration threshold for which a user could receive non-negative

warning time as a function of distance from the source based on alert times in Fig. 4. Color of markers indicate the maximum earthquake magnitude that can be observed by the time of the S-wave arrival, demonstrating that the warnable ground motion is dependent on the earthquake growth at very close distances, and then dependent on 1/R geometrical spreading at farther distances. (Since we use GMPEs for California earthquakes, we cap the maximum magnitude of the source at **M**8.) Horizontal lines indicate distance range for which timely warnings can be issued for each ground motion threshold. The maximum ground motion for which a timely warning can be issued is controlled by the interplay of three factors. First, increasing distance from the source increases the time before the S-wave arrival, giving the EEW system more time to observe more moment release and predict greater ground motion. Second, confoundingly, those predicted ground motion amplitudes decay exponentially with distance from the source. Third, the growth of magnitude, and hence predicted ground motion, is much greater right after initiation than at later times (Fig. 3C). This is because moment increases as t^3, and magnitude is proportional to the logarithm of moment, i.e. magnitude evolution is proportional to the logarithm of time. Since PGA is linearly proportional to magnitude this relation implies that additional increments of seismic moment are less and less efficient in producing strong ground acceleration. Timely warnings can be issued for low thresholds of ground motion for most distances, and timely warnings are rare for high ground motion thresholds. For example, note that only a small near-field distance range can receive timely warnings for 20%*g*, assuming that the strong acceleration occurs with the S-wave arrival. **(B)** Predicted peak acceleration as a function of distance at different times after rupture initiation is shown with colored lines given in 1-s contours (1s and 2s contours labeled for reference). As time increases, more moment is released and thus the predicted acceleration as a function of distance increases. However, magnitude is a logarithmic measure: in the early seconds of the rupture, each second greatly increases the magnitude release and thus the predicted acceleration. But, in later seconds, the growth rate of magnitude (and thus predicted ground motion) decreases precipitously. Annotations on the left side of the color scale show the magnitude that can be estimated at the half-duration time given. Gray region shows ground motions which will always have negative warning times relative to the time of the S-wave arrival. The combination of three factors creates a convex curve for the maximum acceleration for which alerts can be produced before the arrival of the direct S-phase (black line in (B), gray line in (A)). In the near-field, $R<4$ km, and ergo at early times in the rupture process when magnitude growth is most rapid with time, increasing distance allows the user to observe a longer time before the S-wave arrives, which leads to warning for larger ground motions. However, that quickly reverses at distances of 4 km or more, so that the decreasing reward of more observed moment release with increasing distance (and thus increasing time to observe the rupture) is overwhelmed by the exponential decay of ground motion with distance. (This is also seen in the quick peak and subsequent decay of the curve in (A).) Thus there is an upper limit on the maximum warnable ground motion in our hypothetical EEW system, and it is a function of the user's distance from the source (A).

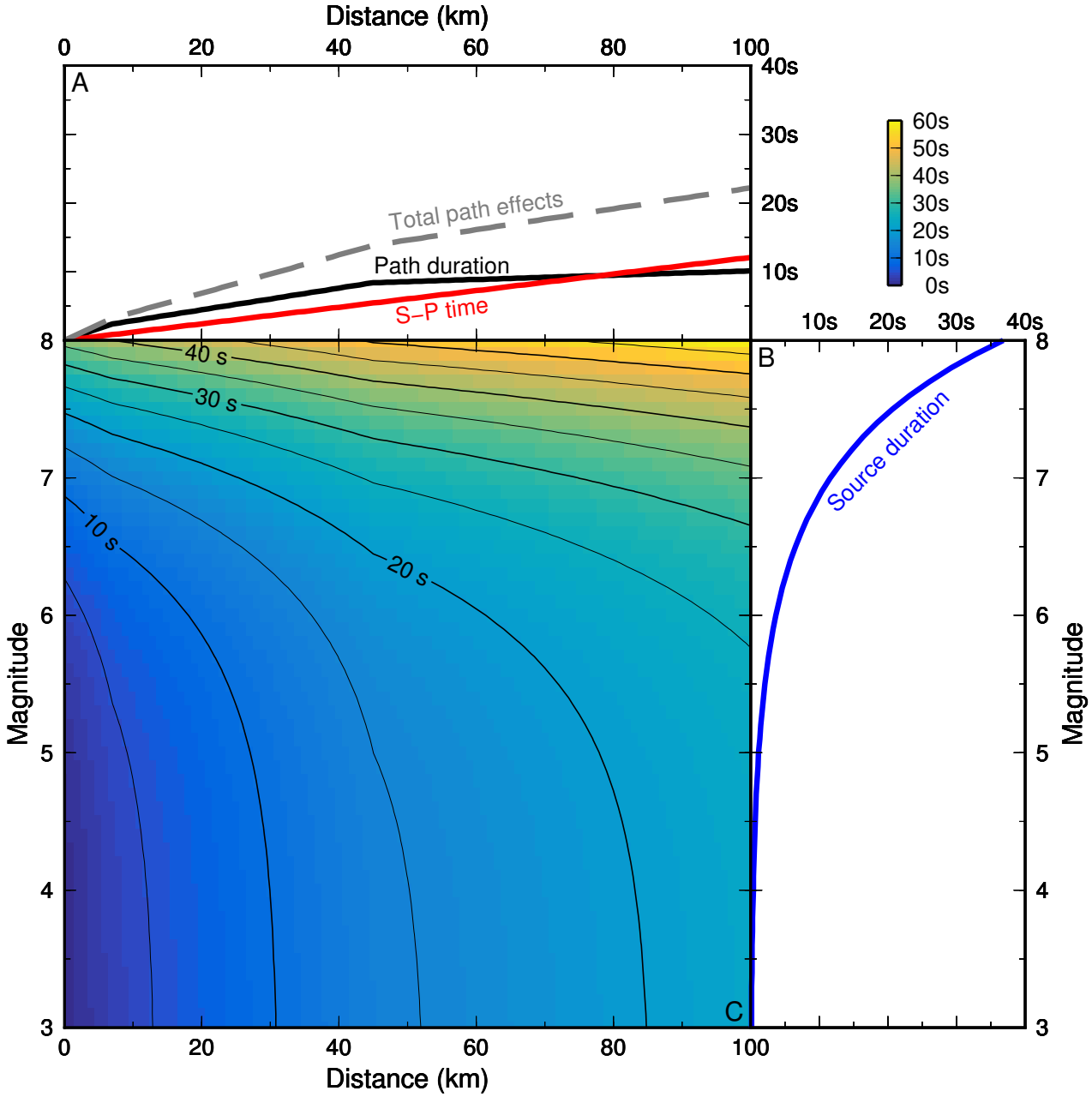

fig. S4. Expected shaking duration as a function of distance and magnitude. (A) Expected path duration, T_{path} (40) and difference between S-wave and P-wave arrivals (S-P time) for a Poisson solid with S-wave velocity of 3.5 km/s. Gray dashed line is the sum of these two quantities, i.e., the total extension of shaking duration as a function of distance from the source. **(B)** Expected source duration, T_d, as a function of magnitude for a circular crack. **(C)** Total expected duration (as a function of distance and magnitude) of shaking from P-wave onset until end of S-wave. This is equal to the sum of the S-P time, T_d, and T_{path}.

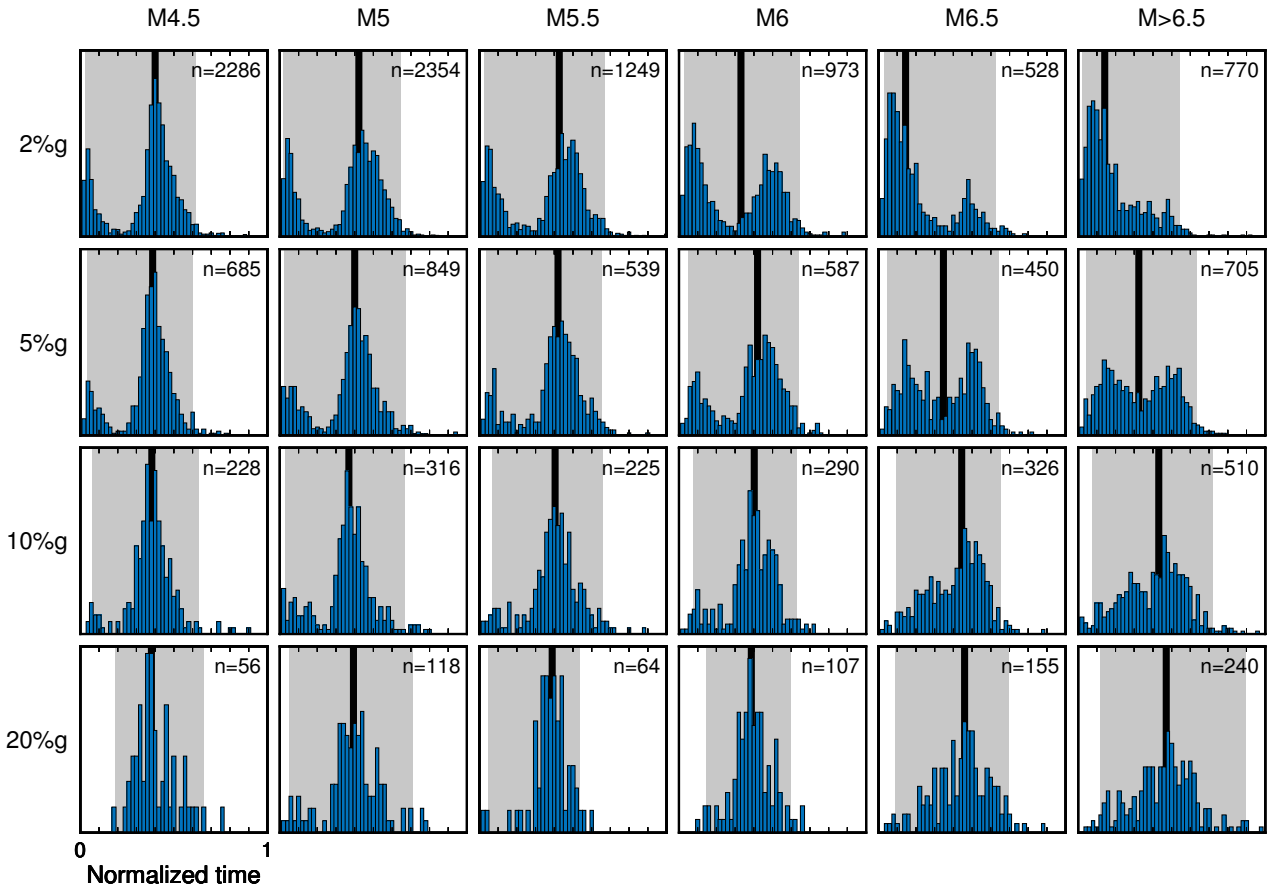

fig. S5. Observed PDFs of time at which specified ground motion threshold is exceeded on the basis of inspection of 48,841 records of M ≥ 4 earthquakes. Exceedance times are normalized by total waveform duration (per Fig. S4) and binned by magnitude. Black line is median time, and gray region shows 95% confidence interval. Number of records is annotated in each subplot. All of the PDFs for the 20%*g* threshold (bottom row) have a simple unimodal shape with the most probable exceedance time occurring during the S-wave. However, progressively lower ground motion thresholds transform these unimodal PDFs to bimodal distributions. Consider the 2%*g* threshold (top row). For small (**M**4.25-**M**4.75) earthquakes (top left subplot), the PDF has two peaks corresponding to the 2%*g* threshold being exceeded in the P-wave and S-wave, respectively. As the earthquake magnitude increases, it becomes more likely that this low threshold of ground motion will be exceeded in the P-wave until, for **M**>6.5 (top right subplot), the PDF becomes unimodal with almost all events exceeding the ground motion threshold before the S-wave arrives.

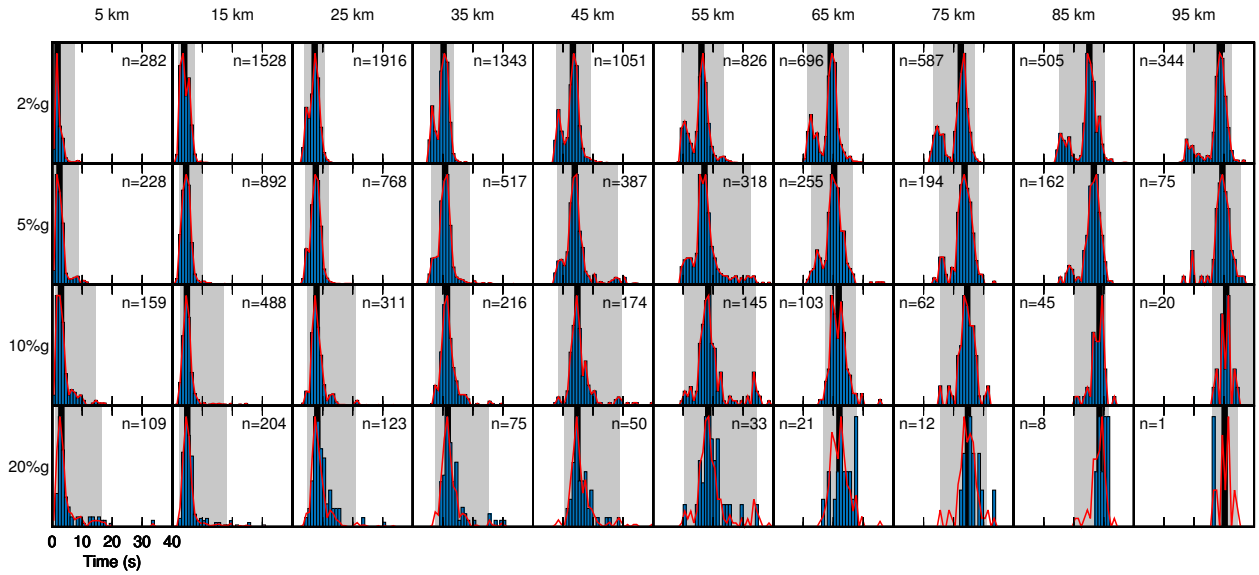

fig. S6. Observed time of exceeding 2, 5, 10, and 20%g from 48,841 records binned by distance. All other symbols are the same as in Fig. S5. Note that PDFs have been normalized to have the same peak amplitude. Because of the scarcity of records exceeding 20%*g*, the PDFs in the bottom row are made from observations of the time of exceeding 10%*g* as well as 20%*g*. The frequency of exceedance times for each threshold is shown by the blue bars. The red lines are the same as the blue boxes for 2%, 5%, and 10%*g*, but in the bottom row are the sum of 10%*g* and 20%*g* observations. As in the previous figure, lower ground motion thresholds are more likely to be exceeded in the P-wave, while higher thresholds are typically not exceeded until after the S-wave onset.

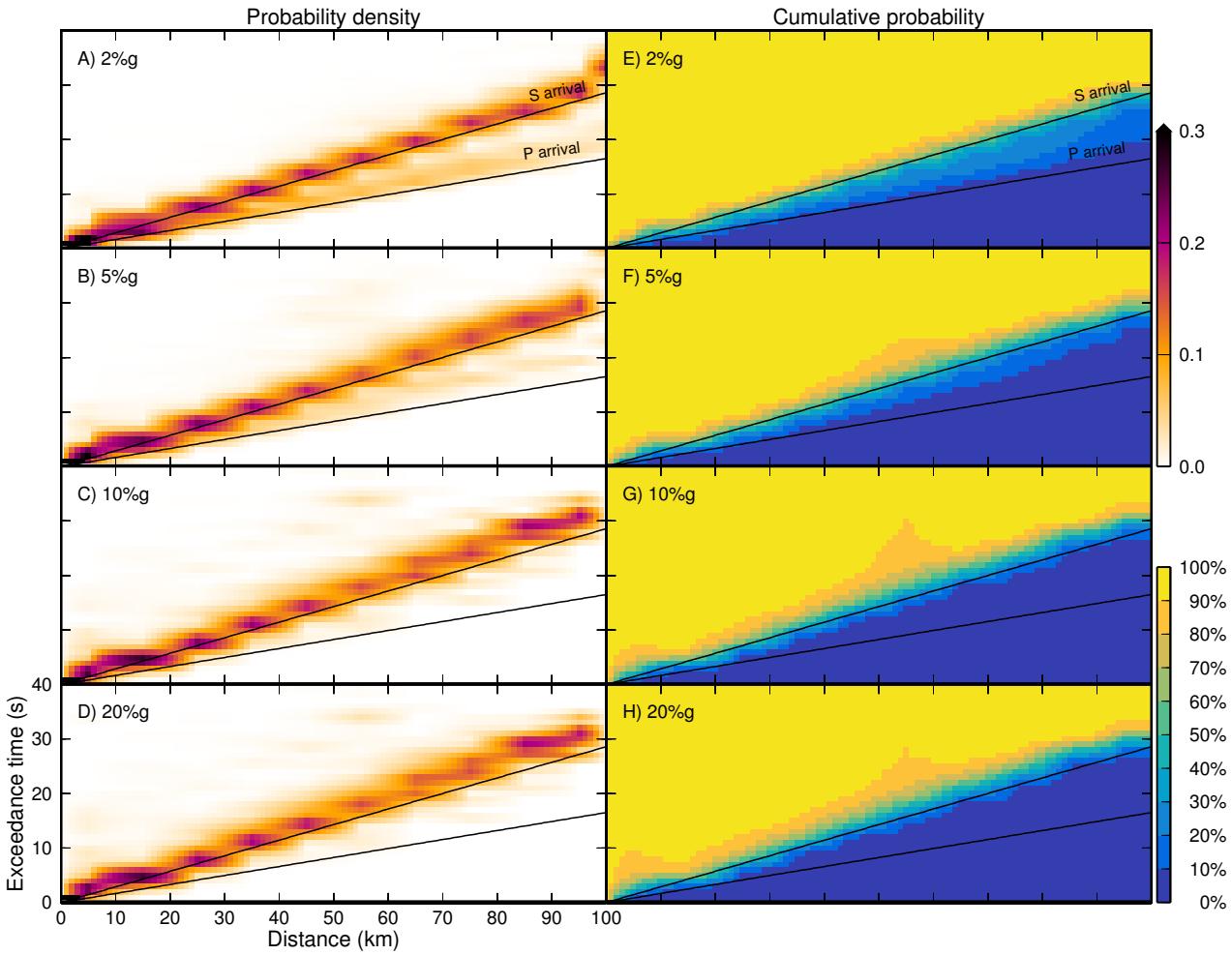

fig. S7. Empirical probability of time that ground motion threshold will be exceeded. All times are relative to origin. Black lines show the P- and S-wave arrival times. **(A-D)** Empirical PDFs of time at which 2%, 5%, 10%, 20%*g* ground motion threshold is exceeded based on 48,841 records. These PDFs are highly peaked immediately following the S-wave arrival shown by the black line, showing that strong ground motion is typically carried by the S-wave, and there is no observational evidence for warning times longer than those presented in Fig. 4. (The warning times in Fig. 4 were based on the assumption that the strong ground motion is carried by the direct S-arrival.) However, note the secondary peak in the PDF between the P-wave and S-wave arrivals for the 2% and 5%*g* thresholds (shown by the high probability density, i.e. bright colors, between the P and S arrivals in A-B particularly). This indicates that these low thresholds of ground motion are often exceeded by the P-wave of large earthquakes, which would significantly decrease the potential warning time to users. **(E-H)** Cumulative probability of exceeding the 2, 5, 10, and 20%*g* ground motion threshold as a function of time after origin based on observed waveforms. These plots are obtained by integrating within each distance bin the empirical PDFs in A-D. Note that even given our large dataset of ~49,000 records, there are not sufficient observations to construct a PDF for all magnitude and distance ranges independently, so instead we considered the arrival times over a normalized duration accounting for source and path effects, equal to the total waveform duration (i.e., S-P time + T_d + T_{path}; Fig. S4). This allows us to aggregate events of different magnitudes, and because the alert times at each threshold are independent of magnitude but dependent on distance (Fig. 4A), we create an empirical PDF of each threshold's exceedance time in 10-km increments of distance. In general, increasingly smaller subsets of these earthquakes reach increasingly larger ground motion thresholds; to make

the statistics robust enough, we grouped the 10 and 20%*g* data together to define the 20%*g* PDFs. (See Fig. S6 for details.)

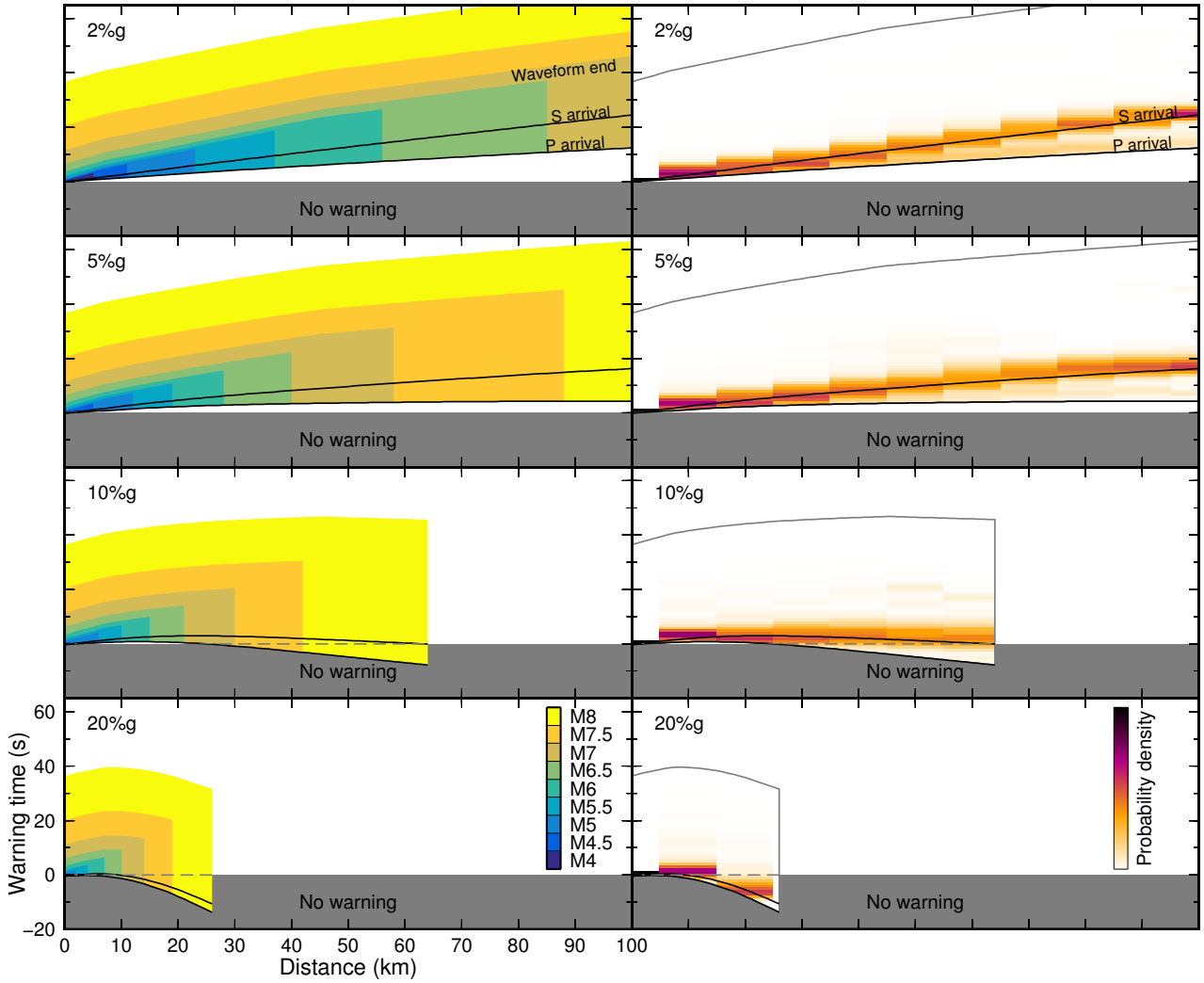

fig. S8. Threshold acceleration warning times for earthquakes of different magnitudes. Left: Each patch is colored by source magnitude and shows the range of warning times the user may experience assuming the strong ground motion happens uniformly at any time between the P-wave arrival and the cessation of shaking. We assume that the total shaking duration is the S-P time + T_d + T_{path} where these quantities are given by the relationships in Fig. S4. Each subplot shows the warning times for a different ground motion threshold. Note that the patches for the smaller magnitudes are plotted on top of those for larger magnitudes. (For clarity, the **M**7 patch is annotated in the first subplot.) The black lines indicate the P and S-wave arrival times. The gray region indicates the cases with negative warning time. Colored patches end at the distance beyond which ground motions are not expected to exceed the user's threshold. Right: Empirical probability based on inspection of ~49,000 records (from Fig. S7) of the arrival times when each threshold of ground motion will be exceeded.

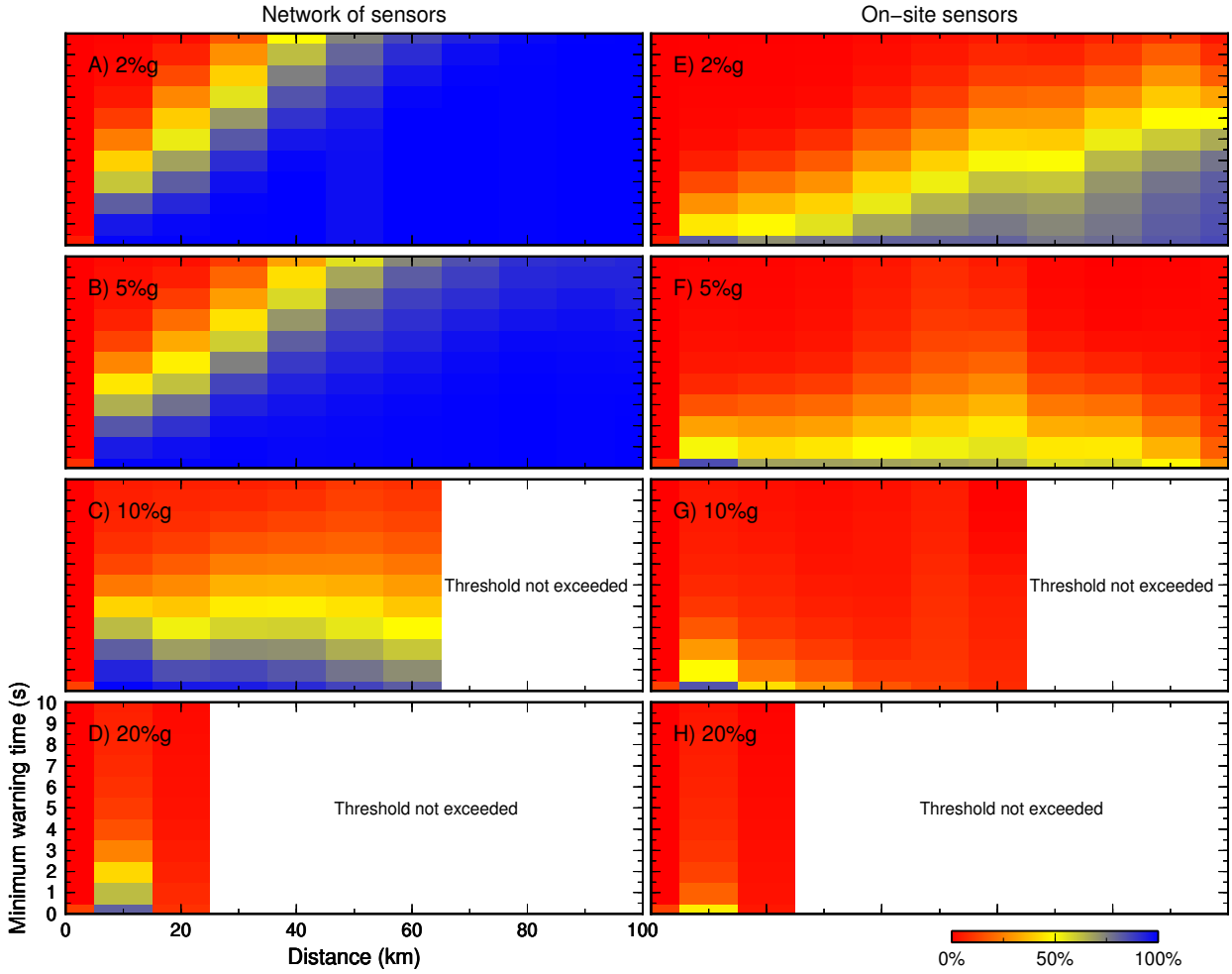

fig. S9. Percentage of events for which users will receive at least a minimum amount of warning time. (A-D) e.g., a user at a distance at 10 km who wishes to receive warning for ground motion of 20%*g* or higher will receive positive warning times for 81% of earthquakes. However, the user may need some minimum amount of time to take protective action. If the user requires at least 3 seconds of warning, that criterion will only be satisfied for 25% of earthquakes. These numbers are obtained by integrating the PDFs in Fig. S8(right). In general, our idealized EEW system can provide long warning times for low thresholds of ground motion, even when accounting for the fact that those thresholds may be exceeded in the P wave (Fig. S7). However, this system can't provide much warning time for strong ground motions: just a second or two for 20%*g* (with a probability of 50%) and only at close distances, and 3 to 5 seconds for 10%*g* at distances from 5 km to 60 km. If a user happens to be in the "sweet spot" for large ground motion thresholds (i.e., greater than 5 km away, but not too far), then a timely warning could be possible. **(E-H)** These plots are the same as (A-D) but for an on-site EEW system that uses data from seismometers placed at the user's location rather than the earthquake source location. Thus, the warning time for each event is reduced by the P-wave propagation time.

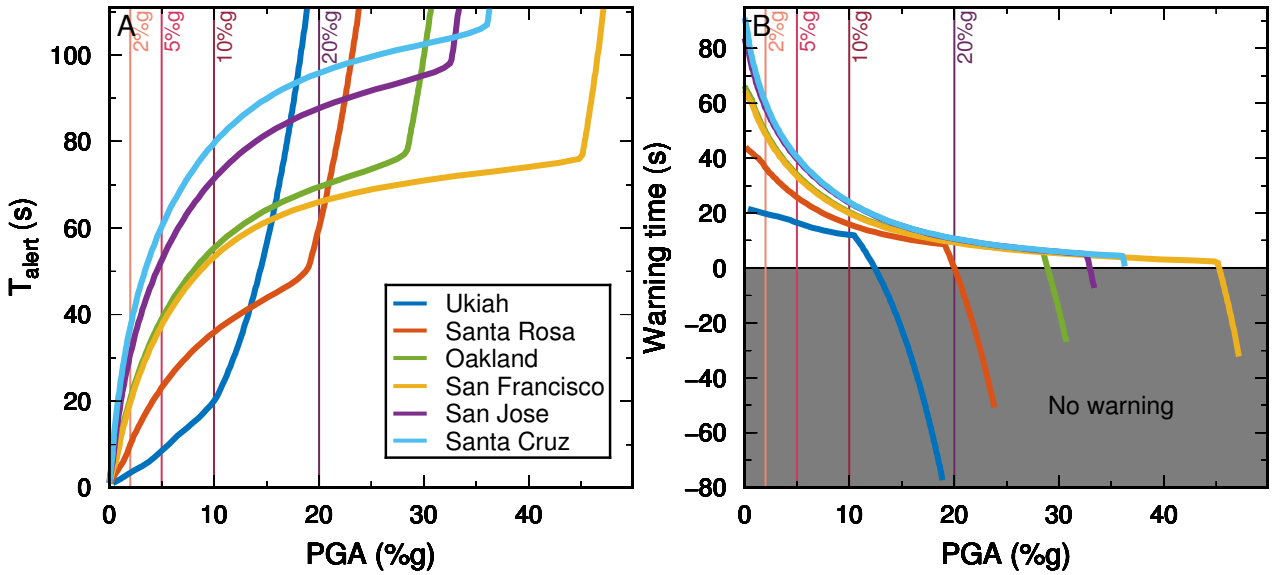

fig. S10. Time required to issue an alert and resulting warning time for the northern San Andreas fault rupture scenario. (A) Time required to issue an alert, T_{alert}, as a function of the ground motion threshold for which the user would like be warned is plotted for each of the six cities shown in Fig. 6. **(B)** Warning time, T_{warn}, assuming that the ground motion threshold is exceeded by the arrival of the S-wave following the indirect travel path shown in Fig. 2. Compare to point source results in Fig. 4. Note that Ukiah is almost behind the rupture and thus sees little effect from the finiteness of the rupture, resulting in alert and warning times similar to those in Fig. 4.